

Complexity based approach for El Niño magnitude forecasting before the “spring predictability barrier”

Jun Meng¹⁺, Jingfang Fan^{1+*}, Josef Ludescher¹⁺, Agarwal Ankit¹, Xiaosong Chen², Armin Bunde³, Jürgen Kurths^{1,4}, and Hans Joachim Schellnhuber^{1*}

¹Potsdam Institute for Climate Impact Research, 14412 Potsdam, Germany

²School of Systems Science, Beijing Normal University, 100875 Beijing, China

³Institut für Theoretische Physik, Justus-Liebig-Universität Giessen, 35392 Giessen, Germany

⁴Department of Physics, Humboldt University, 10099 Berlin, Germany

+these authors contributed equally to this work

*jingfang@pik-potsdam.de or john@pik-potsdam.de

ABSTRACT

The El Niño Southern Oscillation (ENSO) is one of the most prominent interannual climate phenomena. An early and reliable ENSO forecasting remains a crucial goal, due to its serious implications for economy, society, and ecosystem. Despite the development of various dynamical and statistical prediction models in the recent decades, the “spring predictability barrier” (SPB) remains a great challenge for long (over 6-month) lead-time forecasting. To overcome this barrier, here we develop an analysis tool, the System Sample Entropy (SysSampEn), to measure the complexity (disorder) of the system composed of temperature anomaly time series in the Niño 3.4 region. When applying this tool to several near surface air-temperature and sea surface temperature datasets, we find that in all datasets a strong positive correlation exists between the magnitude of El Niño and the previous calendar year’s SysSampEn (complexity). We show that this correlation allows to forecast the magnitude of an El Niño with a prediction horizon of 1 year and high accuracy (i.e., Root Mean Square Error = 0.23°C for the average of the individual datasets forecasts). For the on-going 2018 El Niño event, our method forecasts a weak El Niño with a magnitude of $1.11 \pm 0.23^{\circ}\text{C}$. Our framework presented here not only facilitates a long-term forecasting of the El Niño magnitude but can potentially also be used as a measure for the complexity of other natural or engineering complex systems.

Introduction

ENSO, the interannual fluctuation between anomalous warm and cold conditions in the tropical Pacific, is one of the most influential coupled ocean-atmosphere climate phenomena on Earth^{1–4}. The warm phase of ENSO (El Niño) is characterized by an abnormal warming of the eastern equatorial Pacific, which occurs about every 2–7 years. The Oceanic Niño Index⁵ (ONI) is the primary indicator that the National Oceanic and Atmospheric Administration (NOAA) uses to monitor and identify ENSO events. It is the 3-month running mean of sea surface temperature (SST) anomalies in the Niño 3.4 region ($5^{\circ}\text{S} - 5^{\circ}\text{N}$, $170^{\circ}\text{W} - 120^{\circ}\text{W}$, shown in Fig. 1 as the region inside the pink rectangle). An El Niño event is defined to take place if the ONI is at or above 0.5°C for at least 5 consecutive months (red shades in Fig. 2a). Here we use the value of the highest peak of the ONI during an El Niño event, to quantify its magnitude.

El Niño has been reported to affect the marine ecosystems, commercial fisheries, agriculture, public safety, and to even bring extreme weather conditions in many parts of the globe^{6–14}. Thus the understanding of the underlying mechanism and prediction of El Niño are of great importance for humanity. Numerous models, dynamical as well as statistical ones, were developed to simulate and forecast El Niño events. Dynamical models^{15–24} express mathematically the physical equations of the ocean–atmosphere system. In contrast, statistical model^{25,26} forecasts of El Niño are based on data-driven analyses. During the past decades, the prediction of El Niño has made great progress and skillful forecasts at shorter lead times (up to around 6 months) are possible^{27–29}. However, both types of models reveal very low predictability before and during boreal spring (February–May). This is the so-called “spring predictability barrier” (SPB)^{30–33}.

Recently, several approaches based on climate networks were developed to forecast the onsets of El Niño around one year in advance^{34–37}. One of these approaches³⁴ has correctly forecasted all El Niño onsets or their absence since 2012. However, this method is unable to predict the magnitude of the event. Predicting the magnitude is crucial since a stronger El Niño usually causes more extreme events, e.g., floods, droughts or severe storms, which have serious consequences for economies, societies, and ecosystems. In particular, the El Niño events which started in 1997 and 2014 exhibited relatively high magnitudes and had major impacts on the dynamics and structure of the tropical and temperate ecosystems worldwide³⁸. To fill this gap, here we develop an analysis tool, the *System Sample Entropy* (SysSampEn), to quantify the spatio-temporal disorder degree of

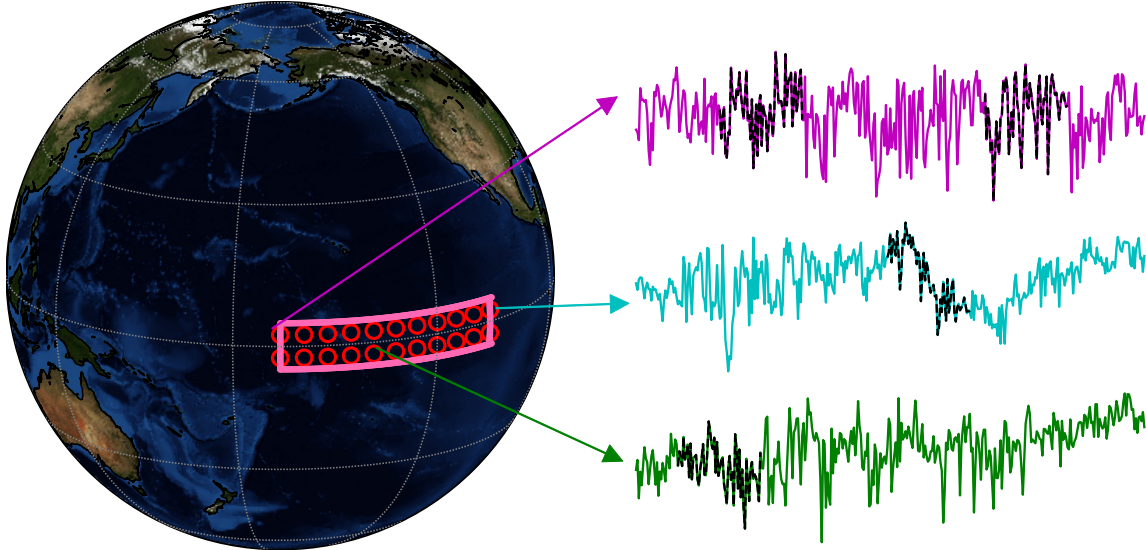


Figure 1. The Niño 3.4 region. The red circles indicate the 22 nodes in the Niño 3.4 region with a spatial resolution of $5^\circ \times 5^\circ$. The curves are examples of the temperature anomaly time series for three nodes in the Niño 3.4 region for one specific year, and several examples of their sub-sequences are marked in black.

temperature variations in the Niño 3.4 region, and to forecast the El Niño magnitude before the SPB. Based on a calendar year's data we forecast, if in the following year an El Niño will start or not. Once the SysSampEn approach forecasted the occurrence of an El Niño onset, we are able to forecast its magnitude with high skill (i.e., correlation $r = 0.84$ and $RMSE = 0.23^\circ\text{C}$ between the forecasted and observed magnitudes for the El Niño events that occurred during the last 35 years). We like to mention that the SysSampEn approach roughly doubles the lead-time at comparable skill. The skill of our El Niño magnitude forecast, based on the previous year's SysSampEn, and thus with a lead-time of about 1 year, is comparable to the best state-of-the-art model forecasts which start in June (i.e., with 6-month lead-time) and predict the same year's boreal winter (November-January) ONI^{39,40}.

System Sample Entropy

We define the SysSampEn for a complex system as a generalization of Sample entropy (SampEn)⁴¹ and Cross-SampEn⁴¹. SampEn was introduced as a modification of approximate entropy^{42,43}. It measures the complexity related to the Kolmogorov entropy⁴⁴, the rate of information production, of a process represented by single time series. The Cross-SampEn was introduced to measure the degree of asynchrony or dissimilarity between two related time series^{41,45}. Both have been widely used in physiological fields, e.g., to make early diagnoses before the clinical signs of neonatal sepsis by analyzing the heart rate variability⁴⁶, to implement an automatic diagnosis of epileptic EEG⁴⁷, and to discriminate different sensory conditions by analyzing human postural sway data⁴⁸.

However, a complex system such as the climate system is usually composed of several related time series (e.g., curves in Fig. 1). Therefore, here we introduce the SysSampEn as a measure of the system complexity, to quantify simultaneously the mean temporal disorder degree of all the time series in a complex system, as well as the asynchrony among them. Specifically, it approximately equals to the negative natural logarithm of the conditional probability that two sub-sequences similar (within a certain tolerance range) for m consecutive data points remain similar for the next p points, where the sub-sequences can originate from either the same or different time series (e.g., black curves in Fig. 1), i.e.,

$$\text{SysSampEn}(m, p, l_{eff}, \gamma) = -\log\left(\frac{A}{B}\right), \quad (1)$$

where A is the number of pairs of similar sub-sequences of length $m + p$, and B is the number of pairs of similar sub-sequences of length m , $l_{eff} \leq l$ is the number of data points used in the calculation for each time series of length l , and γ is a constant which determines the tolerance range. The detailed definition of SysSampEn for an arbitrary complex system composed of N time series is described in the Method section. When $N = 1$, $p = 1$, and $l_{eff} = l$, our definition is equivalent to the classical

SampEn⁴¹. As it is the case for SampEn and Cross-SampEn, before the SysSampEn can be used as an effective tool, appropriate parameter values have to be identified since only certain value combinations can be used to estimate a system's complexity with considerable accuracy. The effective parameter combinations may be different in different complex systems. Here we choose m to be 30 days or 60 days and p to be 15 days or 30 days since El Niño is an interannual phenomenon.

Results

Strong positive correlation between the El Niño magnitude and its previous calendar year's SysSampEn

We calculate the SysSampEn of the climate system composed of the near surface air or sea surface temperature anomaly time series in the Niño 3.4 region and find a strong positive correlation between the El Niño magnitude and the SysSampEn of its previous calendar year (Fig. 2a,b). This positive correlation is significant ($r = 0.90$ on average) and robust across all the analysed datasets (ERA-Interim 1000hPa air temperature⁴⁹ (ERA-Interim), ERA5 1000hPa air temperature⁵⁰ (ERA5), ERA5 sea surface temperature (ERA5 SST) and JRA55-do sea surface temperature⁵¹ (JRA55-do SST)) (Fig. S1).

In the following, we present our results based on the dataset of ERA-Interim, which gives the highest correlation. For a given calendar year between 1984 and 2018, we construct a system composed of temperature anomaly time series in the Niño 3.4 region (see Fig. 1) with a spatial resolution of $5^\circ \times 5^\circ$.

First, we determine the parameter combinations for the SysSampEn, which enable an accurate estimation of the system's complexity. We do this by performing two tests (for details see Method section), which determine, for a given parameter combination, the ability of the SysSampEn to discriminate between higher and lower disordered systems. In the temporal disorder test, we add random numbers to the real temperature data, while in spatial asynchrony test, we compare two systems, one which is constructed from neighboring points on the globe and one which is constructed from randomly chosen points on the globe. An accurate complexity measure should be able to recognize the higher disorder in the more random system and thus assign a higher SysSampEn value to it. We define accuracy as the percentage of correct assignments. Thus, using suitable parameter combinations for the SysSampEn we can quantify the temporal, as well as the spatial disorder in the system.

Surprisingly, we find that the previous calendar year's SysSampEn exhibits a strong positive correlation with the magnitude of El Niño, if the parameter combination for the SysSampEn can quantify the system complexity with good accuracy. Fig. 2c demonstrates on one example, $m = 60$ days and $p = 15$ days, that with changing the values of l_{eff} and γ in Eq. 1, the Pearson correlation (r) between the El Niño magnitude and the previous calendar year's SysSampEn (e.g., blue rectangles in Fig. 2a) increases significantly with the accuracy level. Please note, that the accuracies are calculated fully independently of any El Niño magnitude analyses or forecasts. Thus, the strong correlation between the SysSampEn and the El Niño magnitude is naturally obtained from the parameter combinations, which enable the SysSampEn to quantify the system complexity with high accuracy. In other words, the high predictability of the El Niño magnitude before the “spring predictability barrier” is not the result of overfitting, but it originates from the strong and robust correlation between system complexity and El Niño magnitude.

We also find that the pattern of the SysSampEn between 1984 and 2018 is independent of the data resolution and highly consistent for different parameter combinations which provide high accuracy (Fig. S2 and Table. S1). In particular, the correlation between the El Niño magnitude and the previous calendar year's SysSampEn with different effective ($\geq 95\%$ accuracy level) parameters are all significantly high (the average r is 0.83 ± 0.12), while the best correlation $r = 0.99$ is obtained for $m = 60$ days, $p = 15$ days, $l_{eff} = 345$ days and $\gamma = 9$ (Fig. 2b).

We perform the same analysis on the other datasets and obtain similar results, see Figs. S3-S5 in the SI. We also present in Fig. S1 the scatter plots of the El Niño magnitude versus the previous calendar year's SysSampEn that give the highest r for each of the other three datasets. The correlation r is also significantly high for the other three datasets, and the average r when using all high accuracy parameter combinations of the four datasets (Tables. S1) is 0.79 ± 0.11 . Note that the 2009 El Niño is the only event missed in the onset forecasts (discussed below) and is an exception in the linear relationship.

To obtain the best forecasting performance, we choose the SysSampEn parameters by first conducting an accuracy test and only accepting parameter combinations which lead to a high accuracy (accuracy level $\geq 95\%$ for air temperature and $\geq 85\%$ for SST) in both the spatial asynchrony and the temporal disorder tests. From these high accuracy parameter combinations, we choose in the second step, the one which gives the highest correlation r with the magnitudes of the past El Niño events. We repeat this for all datasets. Table 1 shows the parameters that suggest the highest r for El Niño events before 2018 in the different datasets.

We like to note that, using the old entropy definitions to quantify the system complexity, i.e., calculating the average SampEn per node or the average Cross-SampEn for each pair of nodes in the Niño 3.4 region, we get less significant correlations ($r = 0.42$ on average) than in the SysSampEn approach.

Forecasts of El Niño magnitudes and onsets

Based on the substantial correlations between SysSampEn and El Niño magnitude, we develop efficient hindcasting and forecasting methods for both the El Niño onsets and magnitudes (introduced in the Method section). Then we forecast the

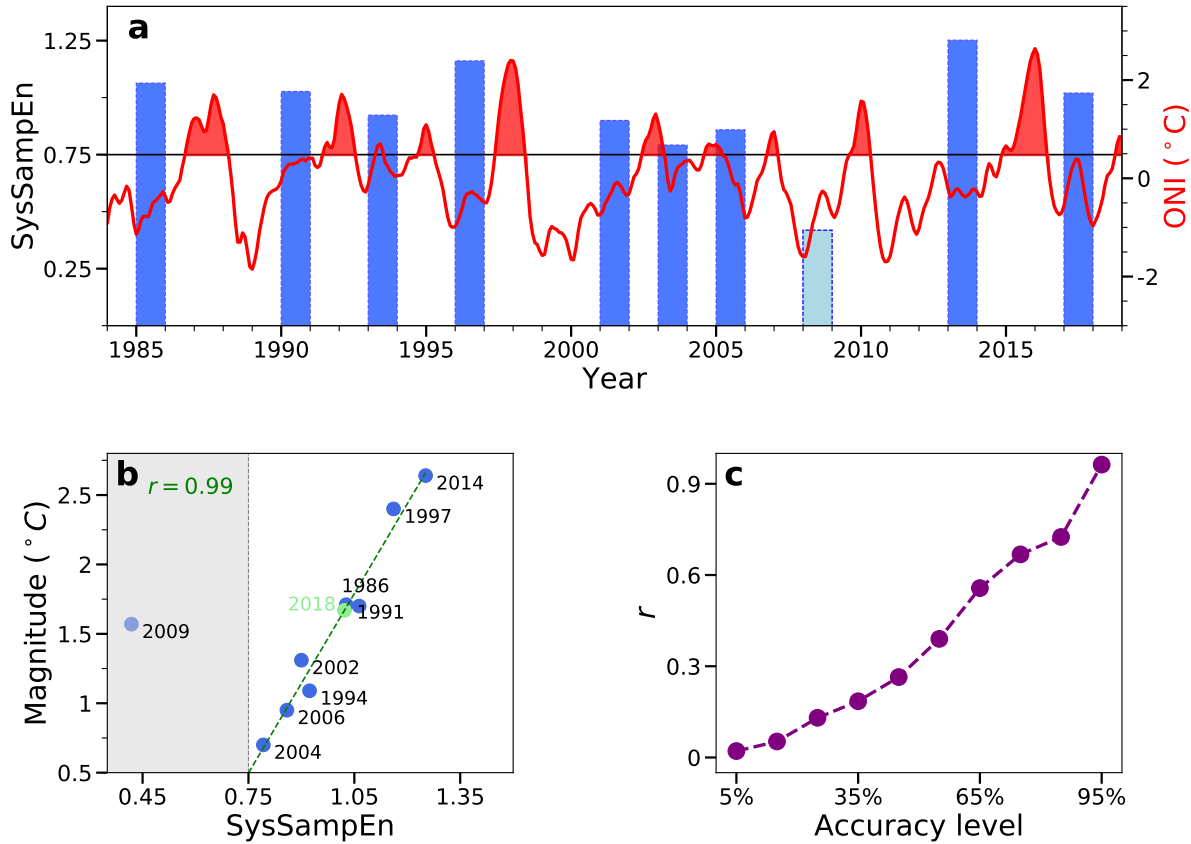


Figure 2. Correlation between SysSampEn and El Niño magnitude. **a** The heights of the blue rectangles indicate the values of the SysSampEn (left scale) for the calendar years preceding El Niño events, calculated from ERA-Interim, by using the set of parameters ($m = 60$ days, $p = 15$ days, $l_{eff} = 345$ days and $\gamma = 9$) that correspond to the highest correlation r with El Niño magnitudes. The red curve is the ONI and the red shades indicate El Niño periods (right scale). **b** Scatter plot of the maximal El Niño magnitude versus previous calendar year's SysSampEn (blue rectangles in **a**). The gray region indicates values of the SysSampEn, which predict for the maximal ONI less than 0.5°C and thus by definition non-El Niño events. The green dashed line shows the best least-square fitted line. **c** The y-coordinate of each purple dot is the averaged correlation r for parameter combinations with accuracy no less than a certain level (i.e., its x-coordinate), in both the spatial asynchrony and the temporal disorder tests. The correlation r between SysSampEn and the El Niño magnitude is monotonously increasing with increasing accuracy level. The calculation of the accuracy level is independent of any El Niño events, thus the strong correlation between the SysSampEn and the El Niño magnitudes emerges naturally without fitting.

magnitude of the ongoing 2018 event, by utilizing the previous calendar year’s temperatures.

To show the high predictability of the El Niño onset before the SPB, we compose a new index (rectangles in Fig. 3a) by substituting the value of the SysSampEn for each calendar year into the best fitting linear functions (green dashed lines in Fig. 2b and Fig. S1), and then taking the average over all the four datasets. Thus the new index has the unit of °C. We find that the value of this index for one specific calendar year can be used to forecast the presence or absence of an El Niño onset in the following year with very good accuracy, i.e., 9 out of 10 correct forecasts of El Niño onsets (dark blue rectangles), with only one missed (pink rectangle); 21 out of 24 correct forecasts of El Niño onset absence years (transparent rectangles), with three missed (gray rectangles). The detailed algorithm is introduced in the Method section.

To demonstrate the high predictability of the El Niño magnitudes before the SPB, we firstly perform leave-one-out hindcasts (described in the Method section) of the magnitudes for all the El Niño events between 1984 and 2017. For each dataset, we use the parameter combination in the function of SysSampEn that gives the highest correlation r between SysSampEn and the magnitudes of the El Niño events before 2018 (Table 1). The observed El Niño magnitudes and hindcasted magnitudes are shown in Fig. 3b. Compared to the real data, we find that our hindcasting method is quite efficient with considerable accuracy, i.e., the root of mean square error (RMSE) = 0.23°C. This indicates that the SysSampEn method has the potential for skillful El Niño magnitudes forecasts with a prediction horizon of 1 year.

Secondly, we perform magnitude forecasts for the 2004, 2006 and 2014 El Niño events by using only data from the event’s past (see Method section), and find that the differences between the observed and forecasted values are within $1 \times RMSE$, see Fig. 3c. These results indicate that $1 \times RMSE$ can be regarded as an error bar. The $RMSE$ is obtained by leave-one-out hindcasting applied only to the regarded events past, e.g., for the 2004 El Niño it depends only on the period 1984-2003. Analogously, the SysSampEn parameters also depend only on the regarded events past and are given in Tables S2-S4. Please note that, for later El Niño events, as more data becomes available for our method, the estimated RMSEs become smaller, see Fig. 3c. The forecast performance for the last 3 El Niño events demonstrates the ability of our method to forecast the El Niño magnitude, as well as providing correct error estimates.

Next, we apply the SysSampEn method to forecast the magnitude of the on-going 2018 El Niño event, based only on data up to 2017. The used SysSampEn parameters are given in Table 1 and obtain for its magnitude 1.11°C, with an error bar of 0.23°C.

DATA			parameter				r	2018(°C)
Type	Name	Resolution	$m(days)$	$p(=q)(days)$	γ	$l_{eff}(days)$		
T 1000hPa	ERA-Interim	5°	60	15	9	345	0.99	1.67
	ERA5	5°	30	30	8	330	0.87	0.58
SST	ERA5	5°	30	30	5	330	0.86	1.09
	JRA-do	4°	30	30	5	360	0.87	1.09
Average							0.90	1.11

Table 1. Values of parameters that suggest the highest correlation between El Niño magnitude and its previous calendar year’s SysSampEn, during the period between 1984 and 2017.

Discussion

We have defined the SysSampEn for complex systems and used it to estimate the spatio-temporal disorder degree of temperature variations in the Niño 3.4 region. We find that a low degree of horizontal synchronization and a high degree of random temporal variations of SST or near surface air temperature are precursors of a strong El Niño. Reliable hindcasts and forecasts of El Niño onsets and magnitudes are achieved for El Niño events that occurred during the last 35 years. Our results reveal a high predictability of both the El Niño onsets and magnitudes already before the boreal spring of the El Niño onset year. For the ongoing El Niño, which started in 2018, our method predicts a weak El Niño with a magnitude of $1.11 \pm 0.23^\circ\text{C}$, based only on data until the calendar year 2017. In addition, from Fig. S2-S5 c, we find that for shorter l_{eff} close to half a year, the correlations between El Niño magnitudes and SysSampEn are still high for certain ranges of parameters. This indicates the possibility for even earlier prediction of El Niño magnitudes, however, with lower prediction skill. This question is left for further studies.

Discussing possible mechanisms related to our findings may help to understand better or even overcome the SPB also in other forecasting models. Here we find some clues from the relationship between near surface ocean turbulence and SST variations⁵³. Recently, it was discovered that strong El Niños are related to intense ocean turbulence, which is characterized by large lateral diffusivity⁵⁴⁻⁵⁶. Enhanced lateral diffusivity during El Niño leads to weaker horizontal temperature gradients and higher horizontal mixing results in lower SysSampEn in the Niño 3.4 region. Our further analyses support our conjecture,

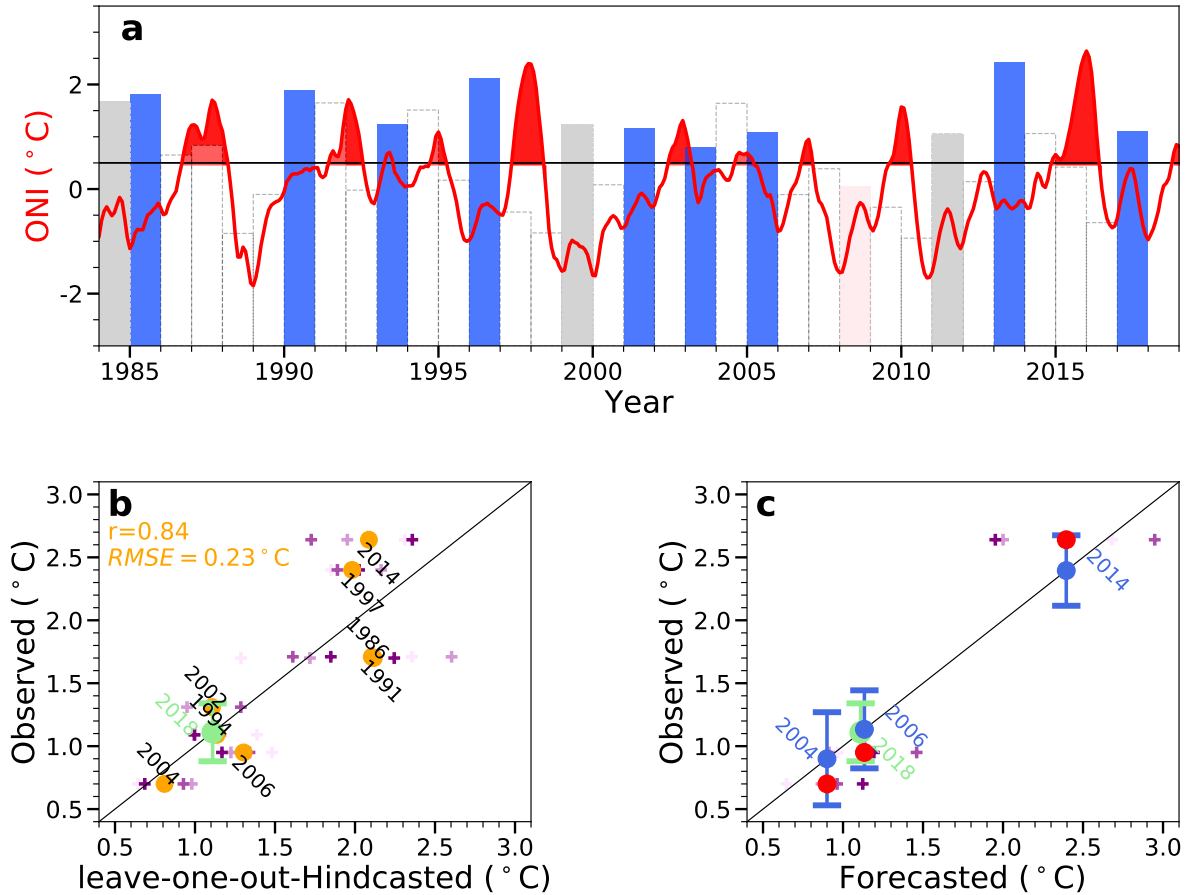


Figure 3. Forecasting the El Niño onsets and magnitudes **a** The value of onset forecasting index (average forecast over the four datasets) is shown as the height of rectangles and is used to forecast the occurrence or absence of an El Niño onset in the following year. If the index value is $\geq 0.5^{\circ}\text{C}$ and the observed ONI in December is below 0.5°C , we forecast the onset of an El Niño in the following year. The blue rectangles show the correctly forecasted El Niño onsets, the pink rectangle indicates a missed El Niño event, the gray rectangles indicate false alarms and the transparent rectangles show when the absence of an El Niño onset was correctly forecasted. **b** Observed temperature versus the leave-one-out hindcasted temperature for the El Niño magnitudes (orange dots) before 2018. The obtained RMSE is 0.23°C . The forecasted magnitude (1.11°C) of the 2018 El Niño event is plotted as a light green dot with an error bar of $1 \times \text{RMSE}$. The “plus” symbols indicate the hindcasted (forecasted) values obtained by using each of the four datasets. **c** Forecasts of the 2004, 2006 and 2014 El Niño magnitudes based only on past information. The error bar for each forecasted El Niño event (blue points) equals $1 \times \text{RMSE}$ (i.e., 0.37°C , 0.31°C and 0.28°C for the 2004, 2006 and 2014 events, respectively) and is calculated from the leave-one-out hindcasts which lie in the regarded events past. Thus, the forecasted value, as well as its error bar (i.e., $1 \times \text{RMSE}$), are only based on the event’s past information. The red dots show the observed magnitudes and are within the error bars. The forecasted 2018 magnitude and its error bar are shown in light green.

as shown in Fig. S6, we find that SysSampEn is inversely proportional to the magnitude of El Niño during El Niño periods. Memory effects have been reported in many natural systems, such as the climate system⁵⁷, physiology^{58,59}, and even in seismic activity^{60,61}. Remarkably, we also observe that there exist memory effects in the dynamical evolution of the SysSampEn, i.e., a smaller SysSampEn is more likely to be followed by a larger one and a larger one follows a smaller one. Fig. S7 demonstrates the SysSampEn of the previous calendar year versus the average SysSampEn of El Niño calendar years (onset calendar year to withdraw calendar year). We argue that during the previous calendar year of a strong El Niño, the near surface lateral diffusivity might be weak, which could be one of the reasons for high SysSampEn in the Niño 3.4 region. However, we think the above hypothesis still needs further analyses based on climate models and observation data. We note that the interannual variability of mesoscale turbulence at the ocean surface has just been found to be regionally correlated with the ENSO indices⁵⁴, which supports our hypothesis. It might be used to explain the relationships among SysSampEn, ocean turbulence, and the El Niño magnitude. Furthermore, we also suspect that the high SysSampEn during the previous calendar year of a strong El Niño is related to the storing of more energy for the event.

The theoretical framework developed here has the potential to improve the El Niño forecasting capability with long lead-time and could also be extended to study and improve our knowledge in other complex systems.

Data

The ERA-Interim archive at ECMWF (<https://apps.ecmwf.int/datasets/>). ERA-Interim (ERA-Interim) is a global atmospheric reanalysis starting from 1979, and is regularly updated. In the present work, we used the zero o'clock daily near surface (1000hPa) temperature, downloaded with a spatial (zonal and meridional) resolution of $2.5^\circ \times 2.5^\circ$. Data for years from 1979 to 2017 were downloaded on October 4, 2018, and data for the last year 2018 was updated on January 29, 2019.

The ERA5 (<https://climate.copernicus.eu/climate-reanalysis>) is a climate reanalysis dataset, developed through the Copernicus Climate Change Service (C3S). It is currently available for the period since 1979 within 3 months of real time. The analysis field of ERA5 has a higher spatial resolution of 31 km and a higher temporal resolution of 1 hour, compared to ERA-Interim. Data used in the present work is the zero o'clock daily near surface(1000hPa) temperature, download on January 25, 2019, and SST downloaded on January 30, 2019, downloaded with a spatial (zonal and meridional) resolution of $2.5^\circ \times 2.5^\circ$.

The JRA55-do (<https://esgf-node.llnl.gov/search/input4mips/>) extends from 1958 to 2018 and is expected to update annually (around April each year). The SST field has a spatial resolution of $1^\circ \times 1^\circ$ and a temporal resolution of 1 day. Data used in the present work is the daily mean SST, downloaded on November 8, 2018, downloaded with a spatial (zonal and meridional) resolution of $1^\circ \times 1^\circ$.

Method

Data Preprocessing

For each calendar year y since 1984 (the first five years 1979-1983 of the datasets ERA-Interim, ERA5 and ERA5 SST, are used to calculate the first anomaly value for 1984), at each grid point α in the Niño 3.4 region, we calculate the anomalies by subtracting the climatological average from the actual temperature and then dividing by the climatological standard deviation. We do this for each calendar day t . For simplicity, leap days were excluded. The calculations of the climatological average and standard deviation are based only on the past data up to the year y .

System Sample Entropy

We first define the System Sample Entropy for an arbitrary system. Let's assume we have N interdependent time series $x_\alpha(t)$ ($\alpha = 1, 2, \dots, N$) of length l composing the system.

1. From each time series, we select sub-records k of length $m < l$, starting at each q -th data point, i.e., starting at $t = k \times q + 1 = 0 \times q + 1, 1 \times q + 1, 2 \times q + 1, \dots$, as long as $k \times q + m \leq l$. Thus a specific sub-records is $X_\alpha^k(m, q) = \{x_\alpha(k \times q + 1), x_\alpha(k \times q + 2), \dots, x_\alpha(k \times q + m)\}$. Then we select n sub-records from each time series and construct a set of $N \times n$ template vectors from the system, i.e., $\Theta(m, q, n) = \{X_\alpha^k(m, q) : 0 \leq k \leq n - 1, 1 \leq \alpha \leq N\}$. We assume that two vectors are close (similar) if their Euclidean distance $d(X_\alpha^i(m, q), X_\beta^j(m, q)) < \gamma \times \max\{\sigma_\alpha, \sigma_\beta\}$ (if $\alpha = \beta$, then $i \neq j$), where σ_α and σ_β are the standard deviations of time series $x_\alpha(t)$ and $x_\beta(t)$ respectively. γ defines the similarity criterion and is a nonzero constant.
2. To examine the probability that two time series which are close at m data points still will be close at the next p data points, we construct analogously another set $\Theta(m + p, q, n)$ by selecting sub-records of length $m + p$. To make the number of template vectors of length m equal to that of length $m + p$, we choose $n \leq \frac{l-m-p}{q} + 1$. In order to reduce the parameter

degrees of freedom and save calculation time, we take $p = q$, then $n \leq \frac{L-m}{p}$. We assume that two template vectors from the set $\Theta(m+p, q, n)$ are close if $d(X_\alpha^i(m+p, q), X_\beta^j(m+p, q)) < \gamma \times \max\{\sigma_\alpha, \sigma_\beta\}$ (if $\alpha = \beta$, then $i \neq j$).

3. The SysSampEn of the system is defined as $SysSampEn(m, p, l_{eff}(n), \gamma) = -\log(\frac{A}{B})$, where A is the number of close vector pairs from the set $\Theta(m+p, q, n)$, B is the number of close vector pairs from the set $\Theta(m, q, n)$, and $l_{eff}(n) = n * p + m$, is the number of days since Jan. 1 of each calendar year, used in the calculation of SysSampEn..

Parameter Determination for the SysSampEn

Here we demonstrate how to determine the $SysSampEn(m, p, l_{eff}, \gamma)$ parameters for our Niño 3.4 climate system by using the ERA-Interim data. For each calendar year, we define a system composed of $N = 22$ (red circles in Fig. 1) temperature anomalies time series $T_\alpha(t)$ ($1 \leq \alpha \leq N$) of length $l = 365$ days.

1. We choose the vector lengths m to be 30 days or 60 days, and the length increases p to be 15 days or 30 days. We focus on a (bi)monthly timescale since El Nino is an interannual phenomenon.
2. The purpose of the SysSampEn is to quantify the spatial and temporal disorder of a given system. This entails, that if we have a spatially and temporally correlated complex system, represented by time series, and add random terms, e.g, white noise, to each time series, then the SysSampEn of the new system should be, with high probability, larger than the original SysSampEn. Similarly, if we replace the times series in a spatially highly correlated system, with unrelated time series, the SysSampEn should increase. We use these properties as the basis of two tests to determine, for given m and p , the values of l_{eff} and γ , which enable a reliable discrimination between more and less ordered systems. For simplicity, we assume γ to be an integer.

- (a) Spatial asynchrony test: For a randomly selected year, we choose randomly three neighboring points on the globe $T_\beta, T_{\beta+1}$ and $T_{\beta+2}$. To construct a highly coupled system, we randomly choose $N = 22$ times one of these three nodes. Thus we obtain a system G_1 with 22 nodes, where $T_\beta, T_{\beta+1}$ and $T_{\beta+2}$ might be present in the system with different frequencies. To contrast, we choose randomly 22 unrelated nodes from the globe to create a system G_2 . We perform this procedure M times. The accuracy is defined as,

$$accuracy = \frac{1}{M} \sum_{i=1}^M S_i, \quad (2)$$

where,

$$S_i = \begin{cases} 1, & \text{for } SysSampEn_{G_2} > SysSampEn_{G_1}; \\ 0, & \text{for otherwise.} \end{cases} \quad (3)$$

In the present study, we used $M = 100$. The accuracy is shown as a function of l_{eff} and γ for $m = 60$, $p = 15$ in Fig. S4 a.

- (b) Temporal disorder test: We compare the SysSampEn of an undisturbed climate system G_1 , here our Niño 3.4 system, with a new system G_2 , where random numbers have been added to the original time series. The new system is composed of $N = 22$ time series $\tilde{T}_\alpha(t) = T_\alpha(t) + R_\alpha(t)$. The $R_\alpha(t)$ are uncorrelated sequences of independent and uniform random numbers in the range $[-0.5 * \sigma, 0.5 * \sigma]$. Here, σ is the average of the $N = 22$ individual time series' standard deviations between Jan. 1, 1984 and Dec.31, 2018. We perform this procedure M times. The accuracy is defined as in Eq. 2 and is shown as a function of l_{eff} and γ for $m = 60$, $q = 15$ in Fig. S4 b.

Forecasting algorithm for El Niño onsets

We forecast the onset of an El Niño event in the following year if the forecasting index (average forecast over the four datasets) is $\geq 0.5^\circ C$ and the observed ONI in December is below $0.5^\circ C$. Otherwise, we forecast the absence of an El Niño onset. The forecasting index is shown in Fig. 3a as the heights of rectangles.

Please note that the forecasting index used in the present work is calculated based on the significant linear relationship between SysSampEn and the magnitudes of El Niño events that occurred in the period 1984-2017. To forecast the occurrence or absence of El Niño onsets after 2018, one should keep updating the forecasting index once a new El Niño has terminated, by choosing the function of the SysSampEn which gives the highest correlation r with the magnitudes of all terminated El Niño events.

Forecasting algorithm for El Niño magnitudes

To forecast the magnitude of an El Niño event starting in the year y ,

- (i) for one dataset, we determine the parameters of SysSampEn by using the ones that give the highest correlation r with the magnitudes of the El Niño events that occurred before the forecasted event y . We regard only parameter combinations which can provide a high accuracy level.
- (ii) for one dataset, we calculate the best fitting line $Y = a * X + b$ between the El Niño magnitude and the previous calendar year's SysSampEn, by using least square regression. Here Y stands the magnitudes of the El Niño events, and X stands the corresponding previous year's SysSampEn. Only past events of the forecasted event y are used in the calculation of the best fitting line.
- (iii) We calculate the SysSampEn in the year $y - 1$, and substitute it into the function of the best fitting line. Then we obtain the expected magnitude of El Niño event starting in the calendar year y .
- (iv) Repeat step 1 and 2 for the other datasets. The forecasted magnitude (blue dots in Fig. 3c) is obtained by taking the average of the four expected magnitudes ("plus" symbols in Fig. 3c).
- (v) To determine the error bar of our forecasting, we perform the following leave-one-out hindcasts for each of the past events of the forecasted El Niño event y :
 - (a) the same as (i).
 - (b) To obtain the leave-one-out hindcasted magnitude of each past event $\bar{y} < y$, we use all events occurred before y except for the hindcasted one to calculate the best fitting line.
 - (c) We calculate the SysSampEn in the year $\bar{y} - 1$, and substitute it into the function of the best fitting line. Then we obtain the expected magnitude of the El Niño event starting in the calendar year \bar{y} .
 - (d) Repeat step 1 and 2 for the other datasets. The leave-one-out hindcasted (orange dots in Fig. 3b) is obtained by taking the average of the four expected magnitudes ("plus" symbols in Fig. 3a).

To forecast the magnitude of the 2018 El Niño event, we substitute for each dataset the SysSampEn value for the year 2017 into the corresponding best fitting linear function, which is determined by all the past El Niño events (except for the 2009 event). Thus we have four individual forecasts, which we average to obtain our final forecast.

References

1. Dijkstra, H. A. Nonlinear Physical Oceanography: A Dynamical Systems Approach to the Large Scale Ocean Circulation and El Niño. (Springer, New York, 2005).
2. McPhaden, M. J., Zebiak, S. E. & Glantz, M. G. ENSO as an Integrating Concept in Earth Science. *Science* **314**, 1740-1745 (2006).
3. Clarke, A. J. An Introduction to the Dynamics of El Niño and the Southern Oscillation. (Academic, London, 2008).
4. Cane, M. A. & Sarachik, E. S. El Niño-Southern Oscillation Phenomenon. (Cambridge University Press, Cambridge, 2010).
5. Oceanic Niño Index (ONI) <https://esrl.noaa.gov/psd/data/correlation/oni.data> (Accessed: March 2019).
6. Ropelewski, C. F. & Halpert, M. S. Global and regional scale precipitation patterns associated with the El Niño/Southern Oscillation. *Mon. Wea. Rev.* **115**, 1606-1626 (1987).
7. Kiladis, G. N. & Diaz, H. F. Global climate anomalies associated with extremes in the Southern Oscillation. *J. Climate* **2**, 1069-1090 (1989).
8. Halpert, M. S. & Ropelewski, C. F. Surface temperature patterns associated with the Southern Oscillation. *J. Clim.* **5**, 577-593 (1992).
9. Diaz, H. F., Hoerling, M. P. & Eischeid, J. K. ENSO variability, teleconnections and climate change. *Int. J. Climatol* **21**, 1845-1862 (2001).
10. Kumar, K. K., Rajagopalan, B., Hoerling, M., Bates, G. & Cane, M. A. Unraveling the mystery of Indian monsoon failure during El Niño. *Science* **314**, 115-119 (2006).

11. Hsiang, S. M., Meng, K. C. & Cane, M. A. Civil conflicts are associated with the global climate. *Nature* **476**, 438-441 (2011).
12. Burke, M., Gong, E. & Jones, K. Income shocks and HIV in Africa. *Econ. J.* **125**, 1157-1189 (2015).
13. Schleussner, C. F., Donges, J. F., Donner, R. V. & Schellnhuber, H. J. Armed-conflict risks enhanced by climate-related disasters in ethnically fractionalized countries. *Proc. Natl Acad. Sci.* **113**, 9216-9221 (2016).
14. Fan, J., Meng, J., Ashkenazy, Y., Havlin, S. & Schellnhuber, H. J. Network analysis reveals strongly localized impacts of El Niño. *Proc. Natl Acad. Sci.* **114**, 7543-7548 (2017).
15. Zebiak, S. E. & Cane, M. A. A model El Niño-Southern Oscillation. *Mon. Wea. Rev.* **115**, 2262-2278 (1987).
16. McCreary, J. P. & Anderson, D. L. T. An overview of coupled ocean-atmosphere models of El Niño and Southern oscillation. *J. Geophys. Res.* **96**, 3125-3150 (1991).
17. Kleeman R. On the dependence of hindcast skill on ocean thermodynamics in a coupled ocean-atmosphere model. *J. Clim.* **6**, 2012-2033 (1993).
18. Kleeman R., Moore, A. M. & Smith, N. R. Assimilation of sub-surface thermal data into an intermediate tropical coupled ocean-atmosphere model. *Mon. Wea. Rev.* **123**, 3103-3113 (1995).
19. Wang, B. & Fang, Z. Chaotic oscillation of tropical climate: A dynamic system theory for ENSO. *J. Atmos. Sci.* **53**, 2786-2802 (1996).
20. Jin, F. F. An equatorial ocean recharge paradigm for ENSO. Part I: Conceptual model. *J. Atmos. Sci.* **54**, 811-829 (1997).
21. Jin, F. F. An equatorial ocean recharge paradigm for ENSO. Part II. A stripped-down coupled model. *J. Atmos. Sci.* **54**, 830-847 (1997).
22. Wang, B., Barcilon A. & Fang, Z. Stochastic dynamics of El Niño-Southern Oscillation. *J. Atmos. Sci.* **56**, 5-23 (1999).
23. Palmer, T. N., et al., Development of a European multimodel ensemble system for seasonal-to-interannual prediction (DEMETER). *Bull. Am. Meteorol. Soc.* **85**, 853-872 (2004).
24. Saha, S., et al., The NCEP Climate Forecast System. *J. Clim.* **19**, 3483-3517 (2006).
25. Xu, J. S. & Storch, H. V., Predicting the state of the southern oscillation using principal oscillation pattern analysis. *J. Clim.* **3**, 1316-1329 (1990).
26. Penland, C. & Magorian, T., Prediction of Niño-3 sea surface temperatures using linear inverse modeling. *J. Clim.* **6**, 1067-1076 (1993).
27. Kirtman, B. P., et al., Current status of ENSO forecast skill: A report to the Climate Variability and Predictability (CLIVAR) Numerical Experimentation Group (NEG), CLIVAR Working Group on Seasonal to Interannual Prediction. *International CLIVAR Project Office, CLIVAR Publication Series No.* **56**, 26 (2002).
28. Chen, D. & Cane, M. A., El Niño prediction and predictability. *J. Computational Physics* **227**, 3625-3640 (2008).
29. Gavrilov, A., et al., Linear dynamical modes as new variables for data-driven ENSO forecast. *Clim. dyn.* **52**, 2199-2216 (2019).
30. Webster, P. J. & Yang, S., The Asian monsoon and predictability of the tropical ocean-atmosphere system. *Quart. J. Roy. Meteorol. Soc.* **118**, 877-926 (1992).
31. Lau, K.M. & Yang, S., Monsoon and ENSO: Selectively interactive systems. *Quart. J. Roy. Meteorol. Soc.* **122**, 945-957 (1996).
32. McPhaden, M. J. Tropical Pacific ocean heat content variations and ENSO persistence barriers. *Geophys. Res. Lett.* **30**, 1480 (2003).
33. McPhaden, M. J. A 21st century shift in the relationship between ENSO SST and warm water volume anomalies. *Geophys. Res. Lett.* **39**, L09706 (2012).
34. Ludescher, J., et al., Improved El Niño forecasting by cooperativity detection. *Proc. Natl Acad. Sci.* **110**, 11742-11745 (2013).
35. Meng, J., Fan, J., Ashkenazy, Y., & Havlin, S. Percolation framework to describe El Niño conditions. *Chaos* **27**, 035807 (2017).
36. Meng, J., Fan, J., Ashkenazy, Y., Bunde, A. & Havlin, S. Forecasting the magnitude and onset of El Niño based on climatenetwork. *New J. Phys.* **20**, 043036 (2018).

37. Nootboom, P. D., Feng, Q. Y., López, C., Hernández-García, E. & Dijkstra, A. Using network theory and machine learning to predict El Niño. *Earth Syst. Dynam.* **9**, 969-983 (2018).
38. Hughes, T. P., et al., Coral reefs in the Anthropocene. *Nature*. **546**, 82 (2017).
39. Barnston, A.G., et al., Skill of Real-Time Seasonal ENSO Model Predictions during 2002–11: Is Our Capability Increasing?. *Bull. Am. Meteorol. Soc.* **93**, 631-651 (2012).
40. Wang, A., Lai, C., Herzog, M. & Graf, H.F., ENSO Forecasts near the Spring Predictability Barrier and Possible Reasons for the Recently Reduced Predictability. *J. Clim.* **31**, 815-838 (2018).
41. Richman, J. S., & Morman, J. R. Physiological time-series analysis using approximate entropy and sample entropy. *Am. J. Physiol.* **278**, H2039-49 (2000).
42. Pincus, S. M. Approximate entropy (ApEn) as a complexity measure. *Chaos* **5**, 110-117 (1991).
43. Pincus, S. M. Quantifying complexity and regularity of neurobiological systems. *Meth. Neurosci.* **28**, 336-363 (1995).
44. Kolmogorov, A. N. New Metric Invariant of Transitive Dynamical Systems and Endomorphisms of Lebesgue Spaces. *Dokl. Akad. Nauk. SSSR* **119**, 861-864 (1958).
45. Pincus, S. M., & Singer, B. H. Randomness and degrees of irregularity. *Proc. Natl. Acad. Sci.* **93**, 2083-2088 (1995).
46. Lake, D. E., Richman, J. S., Griffin, M. P. & Moorman, J. R. Sample entropy analysis of neonatal heart rate variability. *Am. J. Phys. Regul. Integr. Comp. Phys.* **283**, R789-R797 (2002).
47. Acharya, U.R., et al., Automated diagnosis of epileptic EEG using entropies. *Biomed. SignalProcess. Control* **7**, 401-408 (2012).
48. Ramdani, S., Seigle, B., Lagarde, J., Bouchara, F. & Bernard, P. L. On the use of sample entropy to analyze human postural sway data. *Med. Eng. Phys. Med. Eng. Phys.* **31**, 1023-1031 (2009).
49. Dee, D. P. et al. The ERA-Interim reanalysis: configuration and performance of the data assimilation system. *Q. J. R. Meteorol. Soc.* **137**, 553-597 (2011).
50. Copernicus Climate Change Service (C3S) (2017): ERA5: Fifth generation of ECMWF atmospheric reanalyses of the global climate. Copernicus Climate Change Service Climate Data Store (CDS), date of access. <https://cds.climate.copernicus.eu/cdsapp#!/home>.
51. Tsujino, H. et al. *input4MIPs.CMIP6.OMIP.MRI.MRI-JRA55-do-1-3. Version 20180412*. Earth System Grid Federation. <https://doi.org/10.22033/ESGF/input4MIPs.2205> (2018).
52. Supplementary Material.
53. Thorpe, S. A. *An Introduction to Ocean Turbulence*. (Cambridge University Press, Cambridge, 2007).
54. Busecke, J. M., & Abernathey, R. P. Ocean mesoscale mixing linked to climate variability. *Sci. Adv.* **5**, 2375-2548 (2019).
55. Schiermeier, Q., Hunting the Godzilla El Niño. *Nature* **526**, 490-491 (2015).
56. Gnanadesikan, A., Russell, A., Pradal, M. A. & Abernathey, R. Impact of lateral mixing in the ocean on El Niño in a suite of fully coupled climate models. *J. Adv. Model. Earth Syst.* **9**, 2493–2513 (2017).
57. Koscielny-Bunde, E. et al. Indication of a Universal Persistence Law Governing Atmospheric Variability. *Phys. Rev. Lett.* **81**, 729-732 (1998).
58. Peng, C.-K. et al. Long-range anticorrelations and non-Gaussian behavior of the heartbeat. *Phys. Rev. Lett.* **70**, 1343-1346 (1993).
59. Bunde, A. Correlated and Uncorrelated Regions in Heart-Rate Fluctuations during Sleep. *Phys. Rev. Lett.* **85**, 3736-3739 (2000).
60. Livina, V. N., Havlin, S., & Bunde, A. et al., Memory in the Occurrence of Earthquakes. *Phys. Rev. Lett.* **95**, 208501 (2005).
61. Fan, J. et al., Possible origin of memory in earthquakes: Real catalogs and an epidemic-type aftershock sequence model. *Phys. Rev. E* **99**, 042210 (2019).

Data availability

The authors declare that all data which supports the findings are provided with the paper. All data is available from public. Code is available from the corresponding authors upon reasonable request.

Acknowledgements

We acknowledge M. J. McPhaden, S. Havlin, Y. Ashkenazy and N. Marwan for their helpful suggestions. We thank the “East Africa Peru India Climate Capacities — EPICC” project, which is part of the International Climate Initiative (IKI). The Federal Ministry for the Environment, Nature Conservation and Nuclear Safety (BMU) supports this initiative on the basis of a decision adopted by the German Bundestag. The Potsdam Institute for Climate Impact Research (PIK) is leading the execution of the project together with its project partners The Energy and Resources Institute (TERI) and the Deutscher Wetterdienst (DWD).

Author contributions statement

All authors designed the research, analyzed data, discussed results, and contributed to writing the manuscript.

Additional information

Reprints and permissions information is available at www.nature.com/reprints. Correspondence and requests for materials should be addressed to J.F (jingfang@pik-potsdam.de) or H.J.S (john@pik-potsdam.de).

Competing financial interests

The authors declare no competing financial interests.